

Accepted for publication in the Astrophysical Journal

# The Complex Neutral Gas Dynamics Of The Dwarf Starburst Galaxy NGC 625

John M. Cannon

*Department of Astronomy, University of Minnesota,  
116 Church St. S.E., Minneapolis, MN 55455*

cannon@astro.umn.edu

N. M. McClure-Griffiths<sup>1</sup>

*Australia Telescope National Facility, CSIRO,  
P.O. Box 76, Epping, NSW 1710, Australia*

nmmclure@atnf.csiro.au

Evan D. Skillman

*Department of Astronomy, University of Minnesota,  
116 Church St. S.E., Minneapolis, MN 55455*

skillman@astro.umn.edu

Stéphanie Côté

*Canadian Gemini Office, Herzberg Institute of Astrophysics,  
National Research Council of Canada,  
5071 West Saanich Road, Victoria, BC, Canada, V9E 2E7*

stephanie.cote@nrc.ca

## ABSTRACT

We present new multi-configuration H I aperture synthesis imaging of the nearby dwarf starburst galaxy NGC 625 obtained with the Australia Telescope

---

<sup>1</sup>Bolton Fellow

Compact Array. Total H I column density images show gas well-aligned with the optical major axis, and low-column density H I extending to  $> 6$  optical scale lengths. The H I velocity field, on the other hand, is highly disturbed, with neutral gas at nearly all detected velocities within the central region. After considering various interpretations, we find that a blowout scenario most accurately describes the data. Since at our resolution we do not detect any large evacuated holes in the H I disk, we interpret this blowout to be the result of the extended (both spatially and temporally) star formation event which NGC 625 has undergone in the last 100 Myr. This is one of the clearest examples of H I outflow detected in a dwarf galaxy. We find no obvious external trigger for this extended star formation event. We detect strong radio continuum emission from the largest H II regions; comparing to our HST and ground-based H $\alpha$  fluxes suggests either appreciable amounts of extinction toward the star formation regions, or the contribution of non-thermal sources to the radio continuum luminosity.

*Subject headings:* galaxies: evolution — galaxies: irregular — galaxies: starburst — galaxies: dwarf — galaxies: individual (NGC 625)

## 1. Introduction

Nearby dwarf galaxies offer the opportunity to study the dynamics of galaxy evolution at relatively high spatial resolution. In these systems we can probe the nature of star formation and observe its direct impacts on the ISM. Furthermore, the smaller scales of dwarf systems allow us to address the global impacts of starbursts on the ISM, and in relatively high-luminosity cases, the effects on the surrounding IGM as well. In these systems we can attempt to ascertain the triggering mechanisms of starbursts in low-mass galaxies, which will be an important component of models of the chemical and dynamical evolution of galaxies.

As a result of the relative paucity of strong starbursting dwarf galaxies in the local volume, there are few detailed studies of the neutral gas kinematics of such systems. Kobulnicky & Skillman (1995) found the surprising result that in the well-studied dwarf starburst NGC 5253, the large-scale rotation of the galaxy appears to align along the galaxy’s optical major axis. This rare kinematic alignment may be the signature of recent tidal interaction and may provide evidence for a triggered starburst in this system. A more clear case of a triggered starburst is found in NGC 1569. Stil & Israel (2002) find that a low-mass companion seems to be interacting with the system, and that large amounts of the total H I mass are present at unusually high velocities with respect to systemic. These data suggest that infall/outflow and/or tidal effects may be important for this system, and that the current

starburst may present a case of triggered star formation. This burst is having a dramatic effect on the ISM, as turbulent motions appear to support the inner disk, and the mean velocity dispersion is high ( $\sigma_V \sim 20 \text{ km s}^{-1}$ ) compared to other starbursts.

Not all starbursts in low-mass galaxies appear to be tidally induced, however. In NGC 1705, well-known because of its spectacular galactic wind, the global H I kinematics appear to be quite regular (Meurer, Staveley-Smith, & Killeen 1998). While high-velocity H I gas does exist, the kinematics suggest simple rotation and a relatively quiescent velocity field. These few local blue compact dwarfs (BCD’s) support the conclusions of Taylor (1997), wherein it was found that  $\sim 60\%$  of such systems harbor nearby H I companions that may have triggered the current starbursts. However, the local sample also suggests that there must exist another mechanism with which to initiate powerful starbursts in low-mass galaxies. In this investigation we will examine the neutral gas properties of the nearby dwarf starburst galaxy NGC 625, with one of the primary goals being to discern the nature of the triggering mechanism of the current starburst.

The ejection of material from galaxies (i.e., “blowout”) is a topic of great importance for their overall evolution. In systems of decreasing total mass, temporally and spatially concentrated massive star formation becomes increasingly important. For the lowest mass galaxies, “starbursts” can dominate the energetics and luminosity of the system (Dekel & Silk 1986; De Young & Heckman 1994). Such events can also affect their immediate surroundings by injecting energy into the ISM. If the energies are high enough, they can eventually break out of the disk and into the halo, releasing hot gas and processed material which may or may not escape the system entirely to join the surrounding IGM. Numerical simulations of mass loss in low-mass systems (e.g., Mac Low & Ferrara 1999) suggest that it is quite difficult to remove substantial fractions (i.e.,  $\gtrsim 10\%$ ) of the ISM in galaxies with masses  $\gtrsim 10^7 M_\odot$ . Thus it is useful to examine the kinematics of gas in low-mass systems where this model can be empirically tested. As will be discussed below, these observations add NGC 625 to the short list of dwarf systems where neutral gas outflow has been detected.

NGC 625 is an intriguing starburst system located on the far side of the nearby Sculptor Group ( $D = 3.89 \pm 0.22 \text{ Mpc}$ ; Cannon et al. 2003). In that investigation, HST/WFPC2 photometry was used to construct dereddened V vs. (V–I) color-magnitude diagrams. It was found that NGC 625 has been undergoing a prolonged ( $\sim 100 \text{ Myr}$ ) starburst episode. The spatially resolved nature of those data also allowed us to show that the recent star formation has been widespread throughout the central regions. Comparing the locations of young stars with the smooth distribution of older red giant stars, it is likely that star formation has been active for an even longer period. This is one of only a few cases where an extended burst of star formation has been observed in a nearby dwarf galaxy. The

contributing factors to such an evolutionary scenario are not yet fully understood, but the neutral gas dynamics offer us a second avenue with which to investigate the recent evolution of this system.

Previous H I observations of NGC 625 were presented by Côté, Carignan, & Freeman (2000). They identified multiple emission peaks in the central regions of the galaxy and rotation about the galaxy’s optical major axis (as opposed to the typical rotation about the minor axis). The complex kinematics precluded the derivation of a mass model or a rotation curve for this system and prompted the present investigation. As the cause for the complex neutral gas kinematics, Côté et al. (2000) suggest a merger scenario - perhaps with a large H I cloud (which are numerous in this region of the sky, although mostly at differing velocities; see Putman et al. 2002). In a study of the ionized gas kinematics, however, Marlowe et al. (1997) also find complex orbits and motions, suggestive of a major merger as the cause of the burst. The possibility does exist, interestingly, that the kinematics of the ionized and neutral gas are caused by the current burst itself; i.e., perhaps the disk of this system is being disrupted by the strong and extended star formation episode. With these H I data, we seek to further constrain the nature of the recent activity in this system.

Other investigations also point toward the importance of NGC 625 as a nearby example of the dwarf starburst phenomenon. The spectroscopic investigation of Skillman, Côté, & Miller (2003b) finds strong, broad ( $5.5 \text{ \AA}$  EW)  $\lambda 4686 \text{ \AA}$  emission arising from the largest H II region, suggesting a Wolf–Rayet (W–R) classification for the current burst (Conti 1991) and an age of 4–6 Myr. This result is somewhat surprising, given the extended nature of the burst derived in Cannon et al. (2003), and suggests that the presence of W–R features does not necessarily imply a young ( $< 6 \text{ Myr}$ ) burst. Skillman, Côté, & Miller (2003a) find a current star formation rate of  $0.05 \text{ M}_{\odot} \text{ yr}^{-1}$ , comparable to the values found in other high-luminosity dwarf starburst systems. Bomans & Grant (1998) find diffuse 0.1–2.4 keV x-ray emission coincident with the large H II region and extended above the northern side of the plane, suggesting that a galactic wind has been active or has recently terminated. The above properties imply that the recent star formation has been intense in NGC 625; the evolution of this system has been complex and offers an ideal opportunity to study many important questions about the starburst phase of dwarf galaxy evolution. We therefore have begun a multiwavelength study of this system, of which these H I observations form an important part.

For reference, in Table 1 we summarize basic observational properties of this system. We organize this paper as follows. In § 2 we discuss the data obtained and our reductions. The H I data and its analysis, our interpretations, and a simple model are discussed in § 3. In § 4 we discuss the strong radio continuum emission detected from the three highest-surface

brightness H II regions, and § 5 summarizes our conclusions.

## 2. Observations and Data Reduction

We obtained Australia Telescope Compact Array (ATCA)<sup>1</sup> synthesis imaging, utilizing a number of arrays, between 2001 May and 2001 December (see Table 2) for program C968. In total, 75.3 hours were spent on source, with 83 independent baselines sampling UV distances between 0.139 and 27.1 k $\lambda$ . The data were acquired with a correlator configuration that yields two independent datasets: broadband continuum data with total bandwidth of 128 MHz, centered at 1384 MHz, and narrowband spectral line data with 1024 channels, each with an unsmoothed velocity resolution of 0.8 km s<sup>-1</sup>. For the latter, the central observing frequency was 1419 MHz, corresponding to a velocity of 297 km s<sup>-1</sup>. The heliocentric systemic velocity of NGC 625, 413 $\pm$ 5 km s<sup>-1</sup>, corresponds to a frequency of 1418.5 MHz, and thus falls near the center of our spectral observing frequency band. Reductions of each of these datasets followed the standard format, using the MIRIAD<sup>2</sup> package; we briefly summarize the data handling below.

For the continuum observations, interference and bad data were first removed from the UV data. Observations performed with the sun above the horizon were discarded. Bandpass, flux, gain and phase calibrations were then applied, derived from observations of PKS 1934-638 (primary calibrator) and PKS 0201-440 or PKS 0104-408 (secondary calibrators). The calibrated UV data were then imaged and cleaned to produce the continuum map. The resulting image, produced using natural weighting, is discussed further in § 4. The beam size is 6.8'' $\times$ 4.8'', and the rms noise is 38  $\mu$ Jy Beam<sup>-1</sup>. This noise level provides sensitivity to the highest surface brightness H II regions in NGC 625, and we unambiguously detect all three of these sources.

The reduction of the spectral line data is similar to that of the continuum. Imaging produces two spectral cubes for analysis, one of high ( $\sim$  22.5'') and one of low ( $\sim$  45'') resolution, both produced using tapered uniform weighting, and Hanning smoothed to 2.5 km s<sup>-1</sup> velocity resolution. The former will be used to discern the small-scale structure of the high-column density neutral gas, while the latter maximizes our sensitivity to large-scale structure. In the former cube, a typical line-free single-plane rms noise value is 1.1 mJy Beam<sup>-1</sup> (1.55 K), while in the latter it is 2.3 mJy Beam<sup>-1</sup> (0.85 K). We discuss the

---

<sup>1</sup>The Australia Telescope is funded by the Commonwealth of Australia for operation as a National Facility managed by the Commonwealth Scientific and Industrial Research Organisation

<sup>2</sup>See <http://www.atnf.csiro.au/computing/software/miriad>

spectral data in the next section.

### 3. H I Data: Characteristics, Morphology & Kinematics

#### 3.1. H I Characteristics & Morphology

In Figures 1 and 2 we present the total H I emission as derived from zeroth moment calculations from the spectral line data cubes. Figure 1 displays a comparison between the optical galaxy and the extent of the H I at the sensitivity limit of our observations. At the resolution available, the H I in NGC 625 aligns well with the optical galaxy with a low column density extension toward the northwest (also seen in Côté et al. 2000). These observations detect H I to more than 6 optical scale lengths ( $33''$ ; Marlowe et al. 1997). While this is smaller than the extent of the large H I halos seen in some dwarf galaxies (e.g., NGC 4449, Bajaja, Huchtmeier, & Klein 1994; Hunter et al. 1998), the total H I envelope is comparable in size to those of the dwarf and low-surface brightness galaxies in the samples of van Zee et al. (1997) and Côté et al. (2000).

Because the H I distribution ellipticity and orientation agree with those of the optical distribution, one expects a velocity field typical for a dwarf galaxy (i.e., nearly solid-body rotation about the optical minor axis). However, as demonstrated by Côté et al. (2000), the velocity field for NGC 625 is anything but typical. We discuss the velocity structure in detail in § 3.2.

Figure 2 presents zeroth-moment images at both low and high resolution. Both zeroth moment images show a peak column density  $> 2 \times 10^{21} \text{ cm}^{-2}$ . The main H I peak is not coincident with the location of the current major star formation region, but rather is offset to the east by  $\sim 300$  pc. It is interesting to note that we detect a sizable high-column density ( $N_H > 10^{21} \text{ cm}^{-2}$ ) region in the disk. This suggests plentiful dense gas with which to sustain an extended burst of star formation, as was derived in Cannon et al. (2003).

From the low-resolution data cube, we derive a total H I gas mass of  $(1.1 \pm 0.2) \times 10^8 M_\odot$ . We note, however, that there exists significant (maximum  $A_V = 0.57$  mag.) and variable (differences of  $\sim 0.2$  mag. over physical scales of tens of parsecs) extinction in the disk (Cannon et al. 2003), and likely a sizable molecular gas reservoir (Côté, Cannon, & Braine, in preparation), suggesting that the total gas mass is considerably higher than this value. This mass measurement is in good agreement with that found in Côté et al. (2000) after correcting for the new distance found in Cannon et al. (2003).

### 3.2. The Disturbed H I Kinematics

We next examine the velocity structure of the H I gas in NGC 625. In Figure 3 we present individual channel maps from the low-resolution cube. At multiple velocities, the H I gas is multi-peaked, and in some cases (most notably  $429.8 \text{ km s}^{-1}$ ) even forms spatially distinct structures at this sensitivity level. Indeed, as will be argued below, this system appears much more complex in velocity space than the initial distribution and column density images (Figures 1 & 2) would suggest.

A closer examination of the channel maps in Figure 3 shows that NGC 625 is undergoing solid-body rotation about its optical minor axis (i.e., as expected for an inclined rotating disk). However, superposed on this disk are a complex variety of kinematic structures that make the interpretation of the velocity field difficult. Some of this structure (especially at high velocities with respect to systemic) makes the first moment images (see below) appear to contain a component of rotation about the galaxy’s optical minor axis. This unusual behavior, initially posited by Côté et al. (2000), appears to be the result of the superposition of multiple velocity components along the line of sight and not the result of actual rotation about the optical minor axis.

The first moment images (representing intensity-weighted velocity field) are shown in Figure 4. In the low-resolution image, it is clear that many velocity components have been averaged together along the line of sight to form the column density images shown previously. Note in particular the high-velocity gas seen both above and below the H I major axis and the lower-velocity gas seen on both sides of the optical center. The high-resolution velocity field only provides information on the highest-column density H I gas, but there does appear to be agreement in the velocity structure in the regions detected in both the low- and high-resolution velocity fields. Furthermore, solid-body rotation appears to be evident in both cubes, and the high-resolution velocity field shows the central regions less confused with the high-velocity gas above and below the disk as seen in the lower-resolution cube. This very confused velocity structure warrants a further investigation of the nature of the H I emission at all velocities.

In Figure 5 we present five position-velocity cuts along the direction of the optical major axis (position angle =  $90^\circ$ , width =  $3''$ ). One is centered on the H I column density peak, two at  $\pm 30''$ , and two at  $\pm 60''$  north and south of this position (note in Figure 1 the five white lines, which denote the center of each of these PV cuts). Each PV cut is separated by nearly a full beam width. In each section of the figure, note the clear multi-component emission seen at different positions along the cut.

Beginning with the cut through the H I column density maximum (Figure 5c), note

the prominent detection of gas at nearly the full range of velocities ( $360 - 460 \text{ km s}^{-1}$ ) which is coincident with the main body of the galaxy (i.e., within  $1'$  of the central location, and within the optical extent of the system). There is an identifiable, very steep velocity gradient (increasing velocities from negative to positive offsets), which on first inspection might be interpreted as the signature of solid-body rotation of at least part of the H I disk. However, two lines of evidence argue against this. First, under the assumption that this disk is rotationally supported, the implied central mass is  $> 4 \times 10^8 M_{\odot}$ ; i.e., much larger than the kinematic mass of the system (see further discussion in §§ 3.3.1, 3.3.3). Second, and more importantly, the fact that there exists H I at such a wide range of velocities in the central region argues for a highly turbulent disk; this may be a result of the extended and intense star formation event which this system has undergone, depositing energy throughout the disk without the creation of a single massive evacuated cavity as a result. We make further projections on the nature of this gas in the following section. The confused nature of the H I gas in the central regions prevents us from deriving an unambiguous rotation curve for this system.

Next, note the clear detection of two kinematically distinct features in all five PV diagrams, reaching  $> \pm 2'$  from the central position. There is a clear velocity discontinuity at an angular offset of  $-1'$ , where a change of nearly  $100 \text{ km s}^{-1}$  occurs in a very short distance. Similarly, a velocity discontinuity is apparent at an angular offset of  $+1'$ . The symmetry of these features suggests that these are parts of the regularly-rotating H I disk of NGC 625. The high and low-velocity gas both north and south of the central component appears to be superposed on this apparently solid-body rotating component.

The unprecedented structure evident in these PV cuts is a kinematic signature consistent with active blowout of neutral gas from the disk of NGC 625. The presence of H I gas at all velocities in the central sections of the galaxy suggests that large amounts of energy have been deposited into the ISM of this system. Some of the most conspicuous structure is present in the velocity region  $430 - 450 \text{ km s}^{-1}$ , as seen in the panels of Figure 3. This high-velocity gas appears both above and below the optical extent of the system and provides strong evidence for outflow behavior (see § 3.3 for further discussion).

While the strongest tracer of blowout is usually  $\text{H}\alpha$  kinematics, this study adds NGC 625 to the short list of systems where H I blowout is unambiguously detected (see also the Ott et al. 2001 study of Ho-I). Certainly violent star formation has played a role in the evolution of similar systems [e.g., the SMC, Stanimirovic et al. 1999; Ho-II, Puche et al. 1992 (but see also Bureau & Carignan 2002); NGC 1569, Stil & Israel 2002; NGC 1705, Meurer et al. 1998]. While we do not see the small-scale effects of active star formation on the ISM as clearly in NGC 625 as in these other systems (e.g., no clear cases of evacuated shells or chimneys),



it is clear that the current active star formation has had a dramatic effect on the ISM. As we argue in the following section, we interpret this kinematic signature as active blowout of large amounts of H I gas from the disk of NGC 625. This blowout may be the result of the spatially and temporally extended star formation episode which NGC 625 has undergone in the last 100 Myr. Higher-resolution H I imaging would likely show that the active star formation is in the process of evacuating small areas of the ISM. In the next section we consider various interpretations of these PV diagrams.

### 3.3. Possible Kinematic Models for NGC 625

Here we consider a large range of possible interpretations of the disturbed kinematics in NGC 625. In the end, we find that blowout superposed against a disk in nearly solid-body rotation is the only model which successfully reproduces all of the characteristics of the observations. While these data are not of sufficient resolution to detect the small-scale (e.g.,  $< 100$  pc) features of the ISM (where many H I holes and other features may be found), they are more than adequate to examine the nature of the large-scale H I features which are associated with this putative blowout model.

#### 3.3.1. A Simple Rotating Disk

As noted above, the general kinematics of the H I in NGC 625 are consistent with a slowly rotating dwarf galaxy, observed at a relatively high inclination. As seen in Figure 3, the channel maps are consistent with an H I disk that retains strong components of rotation about the galaxy’s optical minor axis. However, superposed on this simple disk model are complicated velocity components that indicate a highly irregular integrated velocity field, and neutral gas at nearly all detected velocities within the H I disk. As can be seen in Figure 5, the simple solid-body behavior is prominent from  $-2'$  to  $+2'$ ; however, in the inner  $\pm 1'$ , the superposition of velocity components interrupts this simple model of the H I distribution. Therefore, these observations are not consistent with *only* a simple H I disk in solid-body rotation. Rather, a more complicated model is required to explain the observations.

### 3.3.2. *Blowout Plus Rotation*

The disk of NGC 625 is seen nearly edge-on. From our HST/WFPC2 observations, the optical axis shows an inclination of  $69^\circ$  (Cannon et al. 2003). Since we cannot unambiguously derive a rotation curve, we cannot derive a precise value for the inclination of the galaxy using these H I data alone. However, using elliptical fits to H I column density contours suggests an inclination of  $(65 \pm 5)^\circ$ . For the purposes of this simple model, we adopt the value of  $65^\circ$  as the inclination of the disk.

Let us assume a “standard” conical blowout emanating from the center of the H I disk (Mac Low, McCray, & Norman 1989; Mac Low & Ferrara 1999). This blowout will push neutral gas preferentially in the direction of lowest pressure; i.e., directly out of the disk (N/S in the case of NGC 625). Assuming this gas breaks out of the H I disk (which should be in solid-body rotation), it will then allow hot gas and metals to be vented into the galactic halo.

In a major-axis position-velocity slice, this scenario will appear similar to Figure 5. More explicitly, the expected solid-body rotation of the H I disk will appear as a diagonal feature, from low velocities and large separation on one side of the disk, to high velocities and large separation on the opposite side of the disk. Superposed on this will be gas of all velocities near the location of the galactic wind center; i.e., at the location of the starburst, we expect to see gas of all velocities, since in a conical blowout model, there will exist some component of velocity along our line of sight from all  $360^\circ$  of the expanding material.

By observing position-velocity diagrams at varying distances from the central disk (here, at different declinations), we should see the solid-body component decrease in strength, while the gas above and below the disk should remain prominent. This is caused by two factors. First, the disk itself is of finite thickness. Thus, the further the distance from the main H I disk, the less neutral gas is involved with the total system rotation. Second, the gas which is being pushed out of the disk should remain visible until the scale height of the blowout. Once this position is reached, the intensity in these features should quickly decrease.

Each of the main points of the blowout scenario is observed in Figure 5. Furthermore, we note that our measure of the inclination is consistent with more H I above the disk than below (compare high and low velocities in the central region cut, and high and low velocities between the  $+60''$  and  $-60''$  cuts). Thus this series of PV diagrams appears to be consistent with a simple picture of a normal dwarf galaxy H I disk, highly inclined with respect to the line of sight, with an internal wind that is causing some of the H I gas to be vented both above and below the plane (with more prominent emission above than below the disk).

### 3.3.3. *Superposed or Counter-Rotating Disks*

Superposed disks (a kinematically distinct small disk rotating in the same sense as a larger disk) have the potential to reproduce the main features of the PV diagram. Here, a large, rotating halo will produce the H I gas detected between  $-2'$  and  $+2'$  in the PV diagram. Superposed on this will be a second component, rotating in the same sense and thus appearing in a similar orientation in the PV diagram. Depending on the difference in mass and rotation speed, the position angle of these two components will vary in the PV diagram. Thus, this model appears to be able to describe the observed PV diagrams.

Upon a closer inspection of Figure 5, however, we can eliminate this possibility because of the size of the components needed. In order to reproduce the observed PV diagram the enclosed mass in the smaller central component would have to be  $> 4 \times 10^8 M_{\odot}$ . This greatly exceeds the masses within the inner 1 kpc found consistently in dwarfs and irregulars, based on mass models of their rotation curves that include gas, stellar and dark matter contributions (e.g., Côté 1995).

The observed PV diagrams are also inconsistent with a counter-rotating disk (e.g., as seen in NGC 4449, Bajaja et al. 1994; Hunter et al. 1998). There, the orientation of the two components (disk and halo) must be in the opposite sense in a major-axis PV diagram; i.e., the direction of increasing velocity for one must be the direction of decreasing velocity for the other. This is opposite to what is observed. Only disks rotating in the same direction can produce the arrangement of features seen in our PV diagram; however, as discussed above, this can only occur with unphysically large central mass concentrations in this low-mass system.

### 3.3.4. *Infall*

In most galaxies it is impossible to distinguish between infall and outflow. If NGC 625 is currently accreting material from a diffuse halo or neighboring H I cloud, this gas could appear as the high-velocity gas near the main H I disk. However, the symmetry of the NGC 625 system is better explained in the context of outflow. If infall were taking place, we would expect to see more gas on one side of a system than the other (e.g., as would result from a merger or from the accretion of a gas cloud). The high-velocity gas (with respect to systemic) seen both above and below the central regions of NGC 625 is more likely exiting the system; because symmetric infall is very rare, this scenario will have difficulty in explaining the observed PV diagrams and velocity field.

### 3.3.5. “Ongoing Assimilation”

Some nearby dwarf irregular galaxies are known to have very extended H I structures with complex kinematics (e.g., IC 10, Shostak & Skillman 1989, Wilcots & Miller 1998; NGC 4449, Hunter et al. 1998). Hunter et al. (1998) invented the phrase “ongoing assimilation” to present a scenario which best describes their present status. In that investigation, large “streamers” of H I gas, highly structured and extending away from the main disk of the galaxy, were posited to be primordial inhomogeneities in the gas cloud surrounding the system that are currently being incorporated into the galaxy. Such a delayed formation scenario had been suggested theoretically (Silk, Wyse, & Shields 1987), and the presence of considerable amounts of diffuse gas in the NGC 4449 halo lends credence to this scenario.

Such a scenario presents an alternative interpretation of these H I observations of NGC 625. Evidence for ongoing assimilation comes from the large amount of diffuse H I surrounding the main galaxy. However, this scenario is not able to explain the complicated velocity structure seen in Figure 5 for two reasons. First, there is no coherent spatial structure in the diffuse H I gas surrounding the galaxy, as seen in NGC 4449. This implies that there has been no “trigger” for the assimilation of the material (which should produce asymmetric structure on large scales), and that we have caught this system in a rare case of activity. Second, and more importantly, the high-velocity gas is seen comparatively close to the main disk of the galaxy, suggesting its energy source is nearby. Unlike NGC 4449, where structures remain coherent in velocity for  $\sim 200 \text{ km s}^{-1}$  and spatially over scales of  $\sim 100 \text{ kpc}$ , the H I in NGC 625 is confined to within  $\sim 50 \text{ km s}^{-1}$  of systemic and to within  $\sim 2.5 \text{ kpc}$  of the optical center of the system. Taken together, these points argue that such a scenario likely cannot explain the structures seen in Figure 5.

### 3.3.6. *Superposed Anomalous-Velocity Clouds*

A chance superposition of two anomalous-velocity clouds could potentially explain the complicated PV diagrams. Indeed, there exist many H I clouds coincident with the Sculptor Group; however, they display a wide velocity dispersion about the systemic velocity of the group, and none are coincident in both position and velocity with NGC 625 (see Putman et al. 2002). While there is a chance that two small clouds have escaped detection in the compilation of Putman et al. (2002), it appears that a chance superposition of two major H I clouds is an unlikely scenario with which to explain the PV diagrams.

### 3.3.7. *ISM Turbulence*

The observed PV diagrams are inconsistent with those expected from a highly turbulent ISM. While there certainly are turbulent processes at work in any area of massive star formation and evolution, it is highly unlikely that such random processes could produce the symmetrical distribution of high-velocity gas near the center of the galaxy. If turbulence were the cause of the high-velocity gas, it would need to remain coherent over spatial scales exceeding a kiloparsec (i.e., the separation between the central PV cut and the cuts at  $\pm 60''$ ). Thus, while turbulence likely has a hand in disturbing the small-scale structure of the ISM in NGC 625, it is highly unlikely that it has produced the high-velocity gas north and south of the disk as seen in the PV diagrams.

## 3.4. Simple Calculation of Burst Energetics

We interpret the complicated velocity structure in NGC 625 as the signature of H I blowout from the disk. However, at our resolution, we do not detect evacuated holes or shells in the disk that would support such a scenario. This implies either that we are witnessing this blowout event relatively early in its evolution, or that the blowout is the result of a continuous, widespread star formation event that has deposited sufficient energy into the ISM to cause H I gas to be expelled into the halo. Given our recent star formation history analysis (see Cannon et al. 2003), we suggest the second scenario is more likely.

Based on the results presented in Cannon et al. (2003), we can estimate the mechanical energy input into the ISM from the recent extended star formation event. In that investigation the authors found a high, but declining, star formation rate over at least the last 100 Myr. More specifically, the average star formation rates over the coarse age bins 0-25 Myr, 25-50 Myr, and 50-100 Myr were found to be 0.008, 0.01 and 0.04  $M_{\odot}\cdot\text{yr}^{-1}$ , respectively. Using these star formation rates, and assuming an IMF, we can estimate the number of SNe that have exploded thus far in this extended star formation event. In particular, we assume a Salpeter IMF, and that all stars above 8  $M_{\odot}$  explode as SNe, each depositing an average of  $10^{51}$  erg of mechanical energy into the surrounding ISM (Burrows 2000).

The results of this simple model suggest that the recent star formation in NGC 625 has deposited  $\sim 10^{55}$  erg of energy in the last 100 Myr. If the total mass of NGC 625 is  $\sim 10^9 M_{\odot}$ , and a scale height of  $\sim 1$  kpc is assumed (roughly the separation between the major H II region and the extent of diffuse x-ray emission; Bomans & Grant 1998), then this amount of energy is comparable to the total gravitational binding energy of the system. Thus the fact that we see kinematic evidence for blowout should not be surprising.

A calculation of the mass of outflowing material is not straightforward. That is, there is no clear kinematic separation between outflowing components and stationary gas within the disk. Rather, it appears that we are viewing a superposition of gas at many velocities along the same line of sight, making it difficult to accurately disentangle gas that is outflowing from gas that is stationary within the disk. However, simple calculations suggest that there has been sufficient energy deposited into the ISM to accelerate a substantial fraction of the neutral gas in this system, with sensible assumptions about the efficiency of mechanical energy deposition. For example, assuming a 20% efficiency for mechanical energy conversion from input SNe energy and a total baryonic mass of  $\sim 10^9 M_{\odot}$  (although note that the dark matter content remains unconstrained from these observations),  $\sim 20\%$  of the H I mass (or  $2.2 \times 10^7 M_{\odot}$ ) could be moved roughly 1 kpc above the disk. Note that a larger dark matter content will decrease the fraction of the H I mass that could be accelerated. Regardless of the mass of material that is currently outflowing, the energetics are more than adequate to account for an outflow scenario.

### 3.5. A Simple Case of Blowout?

As discussed above, we interpret the complex velocity structure in NGC 625 as the signature of blowout, superposed on a normal disk that is undergoing solid-body rotation. This simple scenario offers the best description of the observed PV diagrams. Furthermore, it has been argued that other interpretations of the data have shortcomings that preclude them from accurately reproducing the PV structures.

We note that this interpretation is consistent with other observations of NGC 625. First, using the luminous blue helium burning stars, in Cannon et al. (2003) we derived a recent star formation history where sustained high star formation rates have been maintained for at least the last 100 Myr. While spectroscopic W–R features suggest a much shorter duration for the current burst, the high H I column density shown throughout much of the central disk, and the movement of star formation throughout the disk found in the HST data, suggest that the star formation in this system has been widespread throughout the disk, rather than confined to the location of the current major burst. The 100 Myr timescale would allow large amounts of energy to be put into the ISM, without necessarily leaving one large evacuated cavity which would be detectable at our current resolution. Regardless, we know that there has been an extended period of star formation in NGC 625.

Second, Bomans & Grant (1998) find diffuse soft x-ray emission above the northern side of the disk. This gas shows two x-ray peaks, separated by more than  $1'$ . Based on the

pointing accuracies of ROSAT<sup>3</sup>, we can be sure that this x-ray emission is located in the northeastern halo of the galaxy, and potentially coincident with the disk as well. Given the inclination and the orientation of the outflow which we infer from the PV diagrams, such hot gas ( $T \sim 10^6$  K) would be preferentially seen on the northern side of the disk, i.e., exactly where the diffuse gas is detected. For this hot gas to reach the large distances above the disk where it is seen, an active outflow must have cleared the way for the hot gas to escape. It is possible that the two x-ray peaks correspond to two separate outflow occurrences.

Finally, Skillman et al. (2003a) find chimney-like H $\alpha$  filaments extending radially upward from the galaxy on the northern side (see regions 11 & 12 of their Figure 1). This is exactly what is expected for a blowout scenario, where such chimneys trace the path of hot gas outflow into the halo of the galaxy (Heiles 1993). These low-surface brightness features are clear indicators that a low-density region must have been evacuated to allow unattenuated H $\alpha$  emission to escape to large distances above the disk. Each of these points supports our interpretation of the unusual velocity structure as the signature of blowout from the disk of NGC 625.

Comparing our observational results with the numerical simulations of mass loss in dwarf galaxies in Mac Low & Ferrara (1999), we find good agreement. Our H I mass corresponds most closely to the  $10^8 M_{\odot}$  model presented there. In § 3.4 we estimated the mechanical energy input into the ISM by the recent star formation. The results suggest a scenario comparable to the  $L_{38} = 1-10$  models presented in Mac Low & Ferrara (1999). Examining the gas distributions presented therein, we find that H I is to be expected tens of kpc above and below the disk of the system. Since our H I distribution is smaller than this, we posit that the spatially widespread star formation derived in Cannon et al. (2003) has resulted in outflow, but has deposited this energy throughout the disk, rather than in one spatially concentrated area. Further agreement is found with the x-ray and H $\alpha$  emissivities presented in Mac Low & Ferrara (1999); the diffuse x-ray and H $\alpha$  gas discussed above is consistent with the results for this gas mass and energy input.

#### 4. The Radio Continuum Emission and Extinction Toward the Starburst

Radio continuum emission can be a useful probe of the physical conditions in active star formation regions. In particular, the contribution of non-thermal sources can be identified based on the spectral index of the emission. Via comparison with recombination line intensities (e.g., H $\alpha$ , H $\beta$ ), one can attain a detailed measure of the reddening toward heavily-

---

<sup>3</sup>See the online ROSAT Point Sources Catalogue, <http://wgacat.gsfc.nasa.gov/wgacat/wgacat.html>

obscured star formation regions that would otherwise be inaccessible at optical wavelengths.

The ATCA correlator allows concurrent H I and continuum studies of NGC 625. The broadband continuum data, centered at 1384 MHz, allow a detailed look at the 20 cm radio continuum emission arising from the large H II regions in NGC 625. As shown in Figure 6, we detect strong radio continuum from the largest H II regions (NGC 625 A, B, C of Cannon et al. 2003). The spectroscopic W–R features (Skillman et al. 2003b) arise from the strongest radio continuum source, which is coincident with H II region NGC 625 A.

The total 1384 MHz flux densities from the major H II regions (within apertures the size of, or larger than, the beam) are given in Table 3. Note that H II regions A and D are measured together; since the contribution of D to the combined flux is  $< 4\%$ , this will not affect the results presented here. Following Caplan & Deharveng (1986), for a thermal continuum source in the presence of no extinction, the H $\alpha$  flux and the continuum flux at 1384 MHz are related by:

$$\frac{j_{H\alpha}}{j_{1384}} = \frac{(8.658 \times 10^{-9})(\frac{T}{10^4})^{-0.44}}{(10.486 + 1.5 \cdot \ln(\frac{T}{10^4}))} \quad (1)$$

where  $j_{H\alpha}$  is the flux at H $\alpha$  in  $\text{erg sec}^{-1} \text{cm}^{-2}$ ,  $j_{1384}$  is the flux density at 1384 MHz in Jy, and T is the electron temperature in K. From Skillman et al. (2003b) we adopt an electron temperature for each H II region, listed in Table 3 (note that their H II regions NGC 5, 9 and 18 correspond to NGC 625 A, B, C, respectively, of Cannon et al. 2003). For these parameters we then expect a  $\frac{j_{H\alpha}}{j_{1384}}$  ratio between  $(7.15\text{-}8.04) \times 10^{-10} \text{ erg sec}^{-1} \text{cm}^{-2} \text{Jy}^{-1}$ , for purely thermal emission in the presence of no reddening.

Combining the measured H II region flux densities from the radio continuum with the measured flux of the H II regions based on our previous HST narrowband photometry, we calculate the  $\frac{j_{H\alpha}}{j_{1384}}$  ratio for each of the three most luminous H II regions and use these values to derive the implied  $A_{H\alpha}$ . The low  $\frac{j_{H\alpha}}{j_{1384}}$  values for regions (A+D) and C suggest that either appreciable amounts of extinction exist toward these starburst regions, or that the contribution of non-thermal sources to the radio continuum luminosity is significant. It is very common for  $A_{H\alpha}$  calculated from the ratio of Balmer fluxes to radio continuum fluxes to be much larger than  $A_{H\alpha, \text{Balmer}}$ , even in the absence of nonthermal radio continuum emission (cf. Israel & Kennicutt 1980; Caplan & Deharveng 1986; Skillman & Israel 1986; Bell et al. 2002). This arises simply because in non-homogeneous geometries  $A_{H\alpha, \text{Balmer}}$  can saturate at values as low as 0.4 so that  $A_{H\alpha, \text{Balmer}}$  frequently is only a lower limit to the true extinction. Similar results were found by Beck, Turner, & Kovo (2000) for a sample of Wolf-Rayet galaxies. As shown in Table 3, the extinction varies widely from one H II region



to the next, with region B suffering no extinction as measured from the  $\frac{j_{H\alpha}}{j_{1384}}$  ratio. If the low ratios for regions (A+D) and C are caused by the presence of additional extinction, then these results are consistent with results from both our HST/WFPC2 imaging and ground-based spectroscopy, where strong and variable extinction was found throughout the galaxy. In the latter study, differential extinction precluded a detailed temporal resolution of the recent star formation history.

Unfortunately, with these data we only have one frequency with which to probe the radio continuum, precluding detailed spectral index work to reveal the contribution of potential non-thermal sources. Multi-frequency radio continuum observations of this system are underway (Cannon et al. 2004, in preparation), as they will help to further probe the nature of, and extinction toward, the H II regions in this active dwarf galaxy. We can gain some insight into this issue, however, by using the optical spectroscopy of Skillman et al. (2003b). The  $c(H\beta)$  values calculated therein are converted to  $A_V$  and shown in Table 3. The difference in implied extinctions between the optical (i.e.,  $H\alpha/H\beta$ ) and the radio (i.e.,  $H\alpha$ /radio continuum) suggests that the nonthermal contribution is large; however, multi-frequency data will answer this question definitively. With the current data, we conclude that the measured radio continuum luminosities, when compared to the observed Balmer line fluxes, are consistent with either heavy (and spatially variant) extinction toward some of the starburst regions ( $A_{H\alpha} \sim 1\text{-}2$  mag), or the presence of a large non-thermal component of the radio continuum luminosity.

## 5. Conclusions

We have presented new ATCA multi-configuration H I synthesis imaging of the nearby dwarf starburst galaxy NGC 625. The H I morphology appears smooth on global scales; low-resolution column density images show one strong central H I peak surrounded by a moderate-size low-density halo. However, examining the morphology at higher resolution reveals multiple peaks in the column density, suggesting that the dynamics of the neutral gas are quite complex.

Examination of the velocity field shows a complicated structure, with H I emission detected near the disk across the full velocity range. We find velocity structure in the H I data cubes that appears consistent with the signature of neutral gas blowout from the main disk. While at our resolution we are not sensitive to small-scale structure (which may show holes and other signatures of the influence of massive stars), we are sensitive to the global effects that this star formation is having on the ISM of NGC 625. Because we do not detect large H I holes, and given the results of our HST/WFPC2 star formation history analysis

(Cannon et al. 2003), we prefer the interpretation that the current outflow episode is not the result of one major star formation region, but rather the collective influence of the extended (both temporally and spatially) star formation event which NGC 625 has undergone.

Active blowout is the only interpretation that is capable of reproducing all of the characteristics of the position-velocity diagrams along the major axis of the system. Other potential explanations of the complex velocity structure, including superposed disks, counter-rotating disks, infall, ongoing assimilation, high-velocity clouds, and ISM turbulence, are discussed and rejected, each failing to reproduce all of the observed velocity structure. While a detailed hydrodynamical simulation is beyond the scope of this paper, we encourage further such investigations to better understand the mechanisms involved in creating blowout in low-mass systems.

At the current sensitivity, we find no obvious external trigger for the current burst of star formation. As NGC 625 is a comparatively isolated galaxy, we thus conclude that it has been able to sustain a heightened star formation rate due to the relatively large reservoir of high-column density gas in the central disk regions. The initial triggering mechanism for this extended burst remains unknown.

We detect strong radio continuum emission from the three largest star formation regions in NGC 625. Comparing to our HST/WFPC2  $H\alpha$  fluxes, we find that either appreciable amounts of extinction exist toward these regions, or that there is a strong nonthermal component to the radio continuum emission. We have undertaken multi-frequency continuum observations of this system to further differentiate between these two scenarios.

NGC 625 is a remarkable system. It appears to be one of only a few dwarf galaxies that have shown neutral gas blowout from the active star formation regions. It is the only dwarf galaxy known to show the kinematic signature of blowout, but not to show a large evacuated region near the active star formation region (although such a hole(s) may have gone undetected in the present experiment, at our resolution). Given the detection of diffuse soft x-ray gas above the plane of this system (Bomans & Grant 1998), it appears that the extended massive star formation event in NGC 625 (Cannon et al. 2003) has achieved a similar integrated effect. This has important implications for the evolution of dwarf galaxies. Given the correct conditions, they are able to sustain extended star formation events, which will have dramatic effects on the ISM and surrounding IGM.

The authors appreciate the insightful comments of an anonymous referee that helped to improve this manuscript. J. M. C. is supported by NASA Graduate Student Researchers Program (GSRP) Fellowship NGT 5-50346, and is grateful to the National Radio Astronomy Observatory Foreign Telescope Travel Fund for international travel support. E. D. S.

is grateful for partial support from NASA LTSARP grant NAG5-9221 and the University of Minnesota. This research has made use of: the NASA/IPAC Extragalactic Database (NED) which is operated by the Jet Propulsion Laboratory, California Institute of Technology, under contract with the National Aeronautics and Space Administration; and NASA's Astrophysics Data System.

## REFERENCES

- Bajaja, E., Huchtmeier, W. K., & Klein, U. 1994, *A&A*, 285, 385
- Beck, S. C., Turner, J. L., & Kovo, O. 2000, *AJ*, 120, 244
- Bell, E. F., Gordon, K. D., Kennicutt, R. C., & Zaritsky, D. 2002, *ApJ*, 565, 994
- Bomans, D. J. & Grant, M.-B. 1998, *Astronomische Nachrichten*, 319, 26
- Bureau, M. & Carignan, C. 2002, *AJ*, 123, 1316
- Burrows, A. 2000, *Nature*, 403, 727
- Cannon, J. M., Dohm-Palmer, R. C., Skillman, E. D., Bomans, D. J., Côté, S., & Miller, B. W. 2003, *AJ*, 126, 2806
- Caplan, J. & Deharveng, L. 1986, *A&A*, 155, 297
- Conti, P. S. 1991, *ApJ*, 377, 115
- Côté, S. 1995, Ph.D. Thesis, Mt. Stromlo Observatory
- Côté, S., Carignan, C., & Freeman, K. C. 2000, *AJ*, 120, 3027
- De Young, D. S. & Heckman, T. M. 1994, *ApJ*, 431, 598
- Dekel, A. & Silk, J. 1986, *ApJ*, 303, 39
- Heiles, C. 1993, *Reviews of Modern Astronomy*, 6, 19
- Hunter, D. A., Wilcots, E. M., van Woerden, H., Gallagher, J. S., & Kohle, S. 1998, *ApJ*, 495, L47
- Israel, F. P. & Kennicutt, R. C. 1980, *Astrophys. Lett.*, 21, 1
- Kobulnicky, H. A. & Skillman, E. D. 1995, *ApJ*, 454, L121
- Mac Low, M. & Ferrara, A. 1999, *ApJ*, 513, 142
- Mac Low, M., McCray, R., & Norman, M. L. 1989, *ApJ*, 337, 141
- Marlowe, A. T., Meurer, G. R., Heckman, T. M., & Schommer, R. 1997, *ApJS*, 112, 285
- Meurer, G. R., Staveley-Smith, L., & Killeen, N. E. B. 1998, *MNRAS*, 300, 705
- Ott, J., Walter, F., Brinks, E., Van Dyk, S. D., Dirsch, B., & Klein, U. 2001, *AJ*, 122, 3070

- Puche, D., Westpfahl, D., Brinks, E., & Roy, J. 1992, *AJ*, 103, 1841
- Putman, M. E. et al. 2002, *AJ*, 123, 873
- Schlegel, D. J., Finkbeiner, D. P., & Davis, M. 1998, *ApJ*, 500, 525
- Shostak, G. S. & Skillman, E. D. 1989, *A&A*, 214, 33
- Silk, J., Wyse, R. F. G., & Shields, G. A. 1987, *ApJ*, 322, L59
- Skillman, E. D., Côté, S., & Miller, B. W. 2003a, *AJ*, 125, 593
- Skillman, E. D., Côté, S., & Miller, B. W. 2003b, *AJ*, 125, 610
- Skillman, E. D. & Israel, F. P. 1988, *A&A*, 203, 226
- Stanimirovic, S., Staveley-Smith, L., Dickey, J. M., Sault, R. J., & Snowden, S. L. 1999, *MNRAS*, 302, 417
- Stil, J. M. & Israel, F. P. 2002, *A&A*, 392, 473
- Taylor, C. L. 1997, *ApJ*, 480, 524
- van Zee, L., Haynes, M. P., Salzer, J. J., & Broeils, A. H. 1997, *AJ*, 113, 1618
- Wilcots, E. M. & Miller, B. W. 1998, *AJ*, 116, 2363

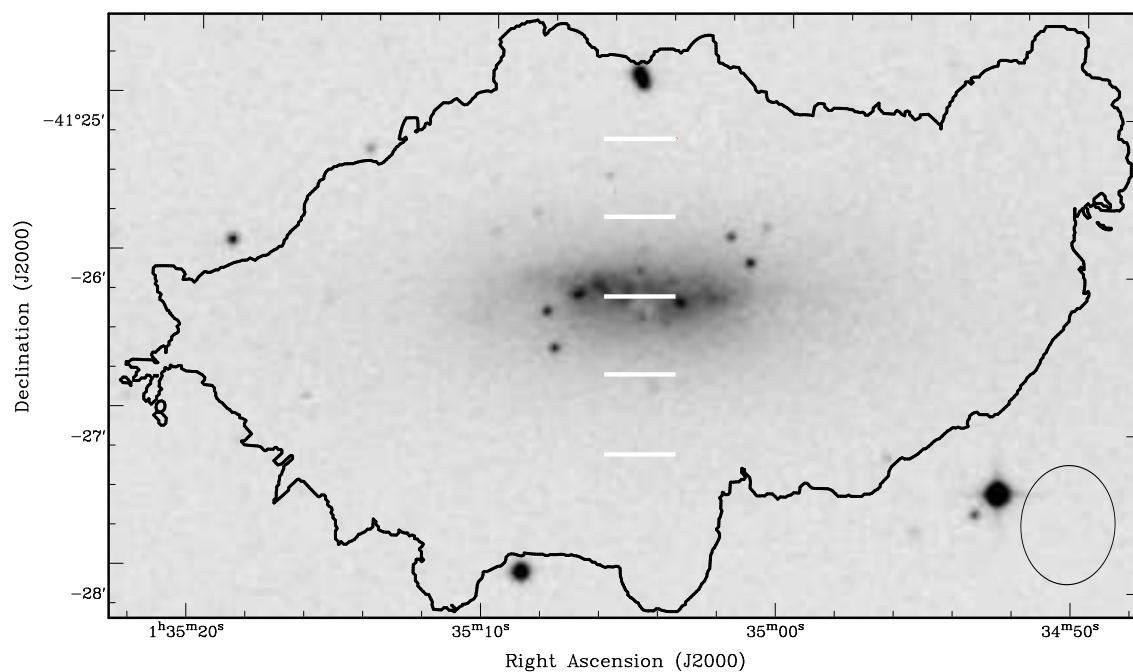


Fig. 1.— POSSII near-infrared image of NGC 625 overlaid with the lowest contour of the zeroth-moment (total H I column density) image presented in Figure 2. This sensitivity limit corresponds to a column density of  $1.56 \times 10^{19} \text{ cm}^{-2}$ . The neutral gas is highly extended in this system; H I is strongly detected to  $\sim 6$  optical scale lengths (Marlowe et al. 1997). The major star formation region is evident on the eastern side of the main disk (see also Figure 6).

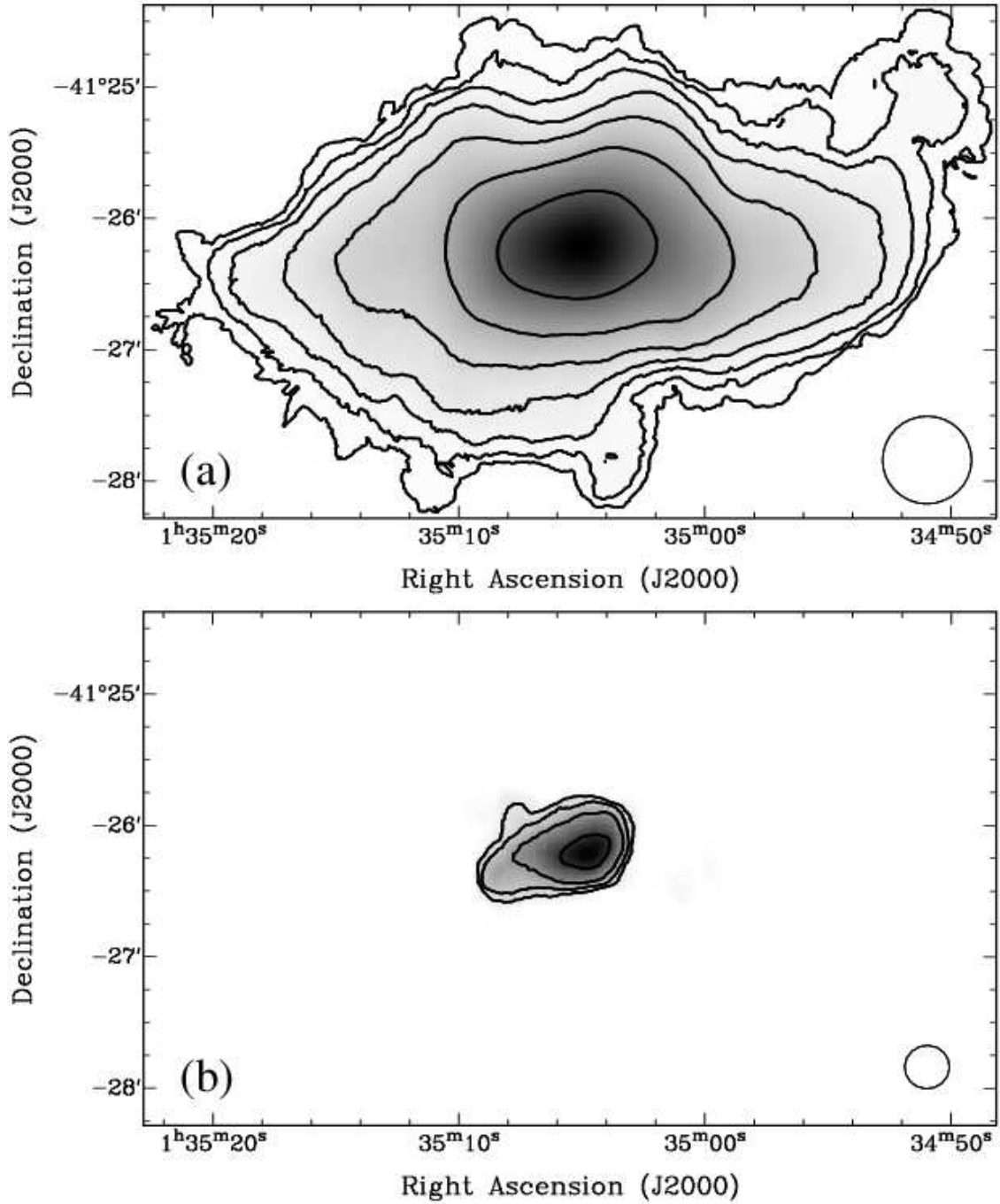


Fig. 2.— Velocity-integrated zeroth-moment images, representing total H I column density. (a) shows the low-resolution ( $45''$  beam) image, while (b) shows the higher-resolution ( $22.5''$  beam) image. Contours in (a) show levels of 1, 2, 4, 8, 16, 32 and 64% of the peak intensity ( $1178 \text{ K}\cdot\text{km s}^{-1}$ , or  $2.15 \times 10^{21} \text{ cm}^{-2}$ ), while the contours in (b) show levels of 10, 20, 40 and 80% of the peak intensity ( $1321 \text{ K}\cdot\text{km s}^{-1}$ , or  $2.41 \times 10^{21} \text{ cm}^{-2}$ ). The beam size and shape is shown at the bottom right of each image.

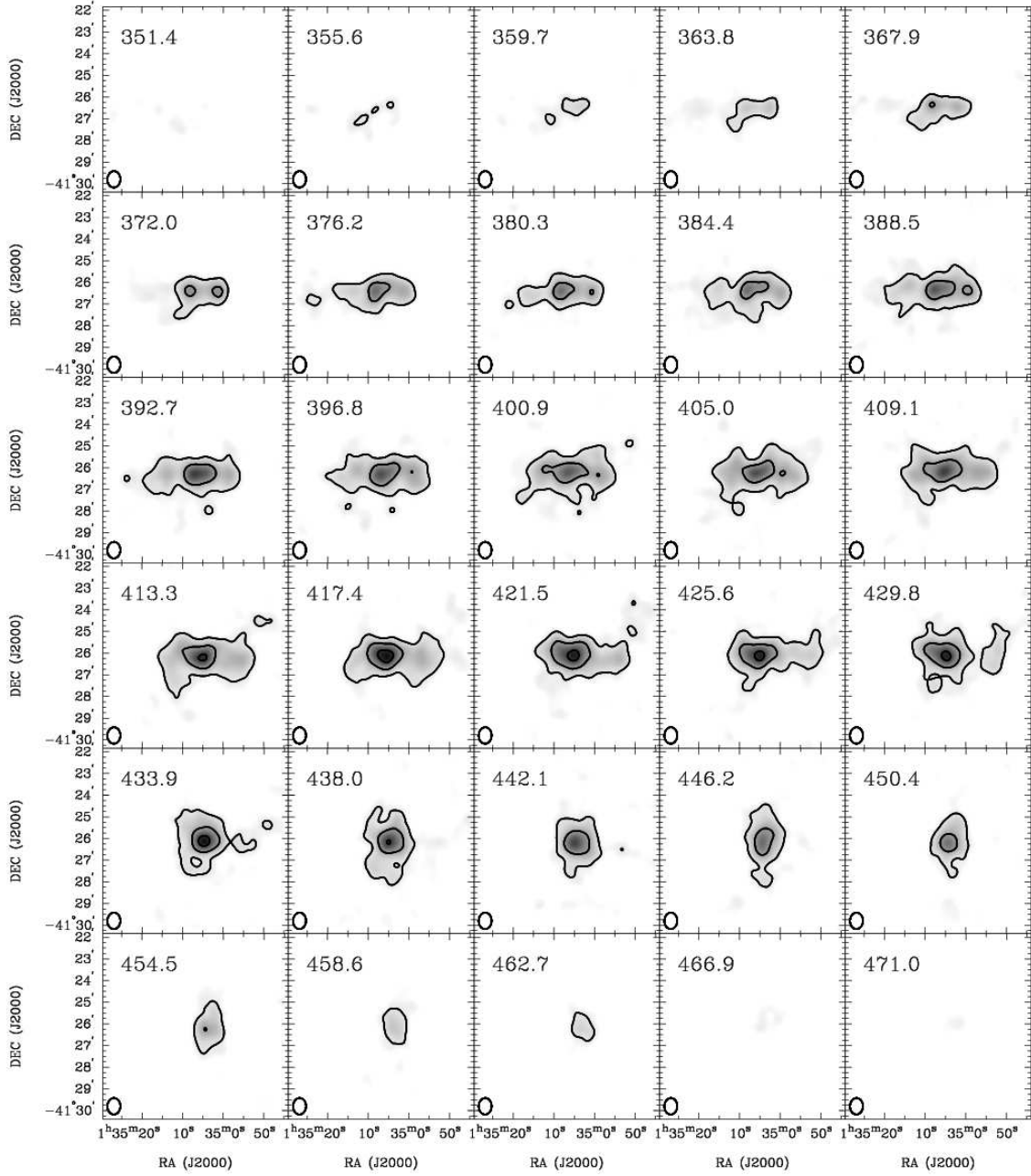


Fig. 3.— Low-resolution ( $45''$  beam) H I data showing planes of constant velocity, as labeled in the upper left corner of each frame. The image stretch is linear, from the noise level ( $2.3 \text{ mJy Beam}^{-1}$  in line-free individual planes) to the maximum intensity of  $53 \text{ mJy Beam}^{-1}$ . The contours show levels of 3, 9, and 18 sigma, corresponding to  $1.18$ ,  $3.54$ , and  $7.08 \times 10^{19} \text{ cm}^{-2}$ , respectively. The figure shows three-channel averages, separated by 5 increments of the unsmoothed velocity resolution of  $0.8 \text{ km s}^{-1}$ .



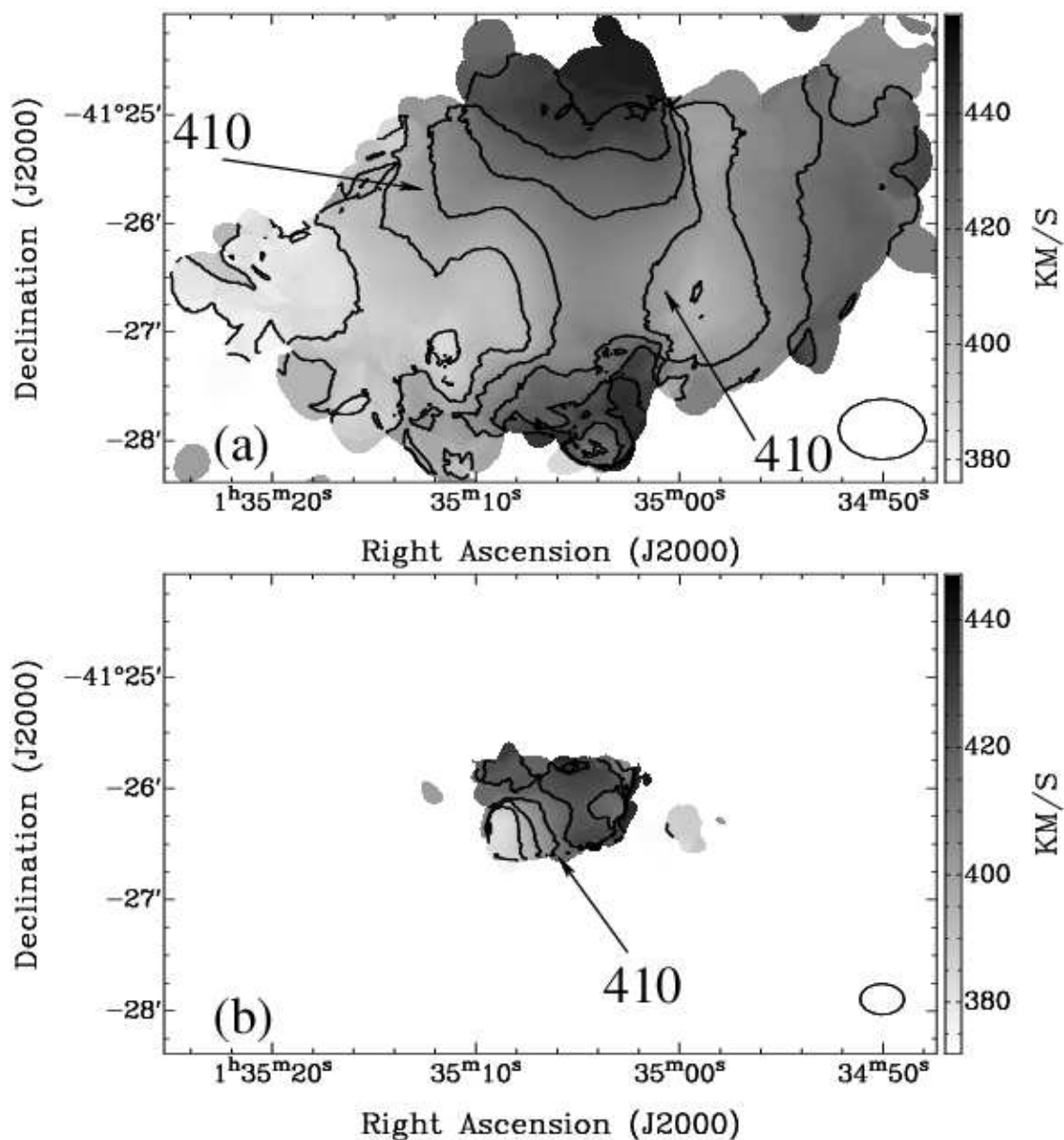


Fig. 4.— Velocity-integrated first-moment images, representing radial velocity. (a) shows the low-resolution (45'' beam) velocity field, while (b) shows the higher-resolution (22.5'' beam) velocity field. The contours are spaced by  $10 \text{ km s}^{-1}$  intervals, ranging from  $380 \text{ km s}^{-1}$  to  $440 \text{ km s}^{-1}$  in (a) and from  $380 \text{ km s}^{-1}$  to  $430 \text{ km s}^{-1}$  in (b). The velocity field is highly disturbed, with components across the full velocity range within the disk, as well as components with steep velocity gradients.

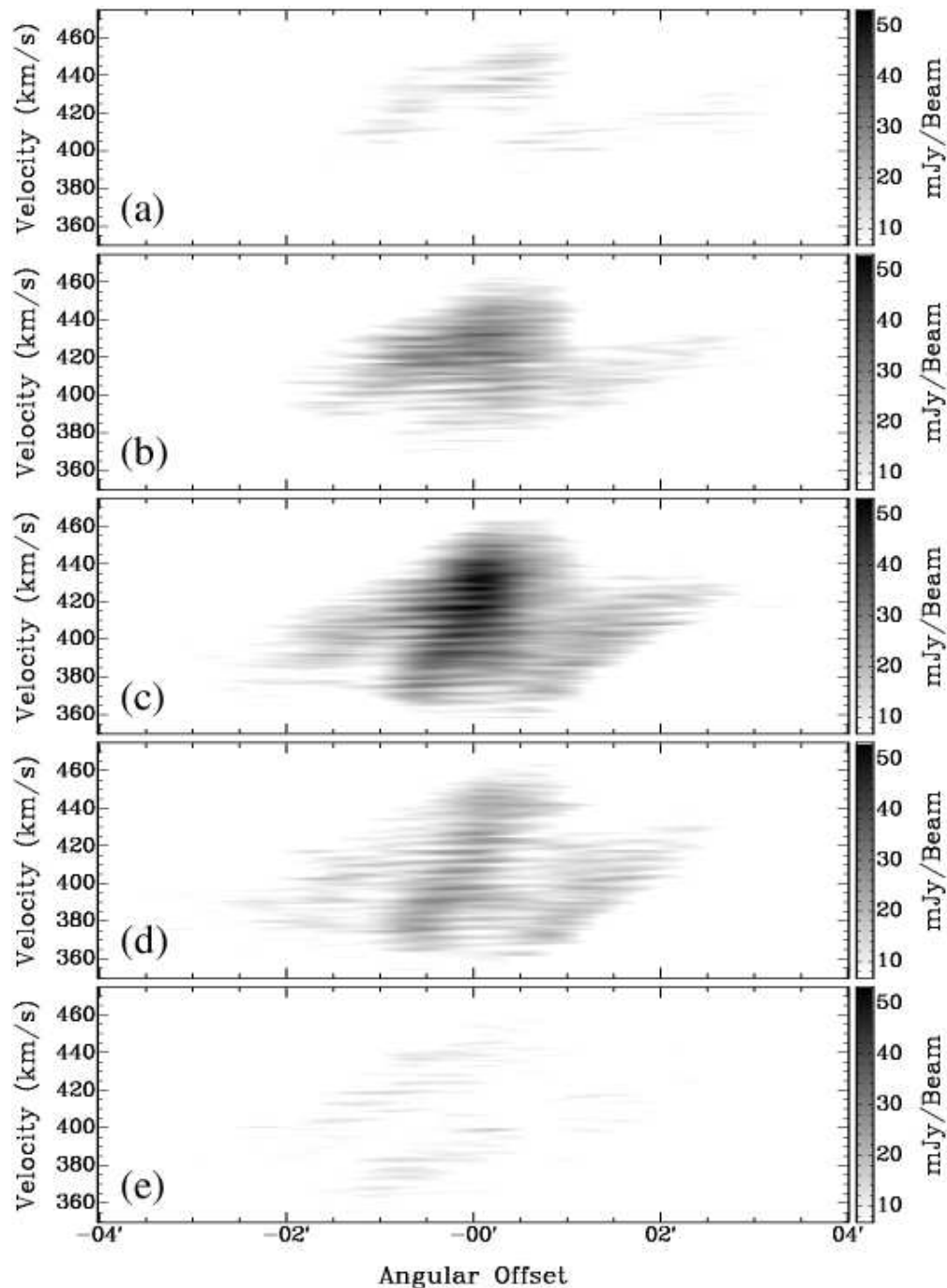


Fig. 5.— Five independent major-axis PV diagrams, taken at different distances from the H I column density maximum, located at  $\alpha, \delta$  (J2000) = 01:35:4.93,  $-41:26:12.20$ . (a) is located  $60''$  N of the disk, (b) at  $30''$  N, (c) coincident with the H I peak, (d) at  $30''$  S, and (e) at  $60''$  S. Each of these locations is shown by a small white line in Figure 1. The cuts are  $8'$  long, at a position angle of  $90^\circ$ . Near the disk, the kinematic signature of blowout dominates the H I velocity structure.

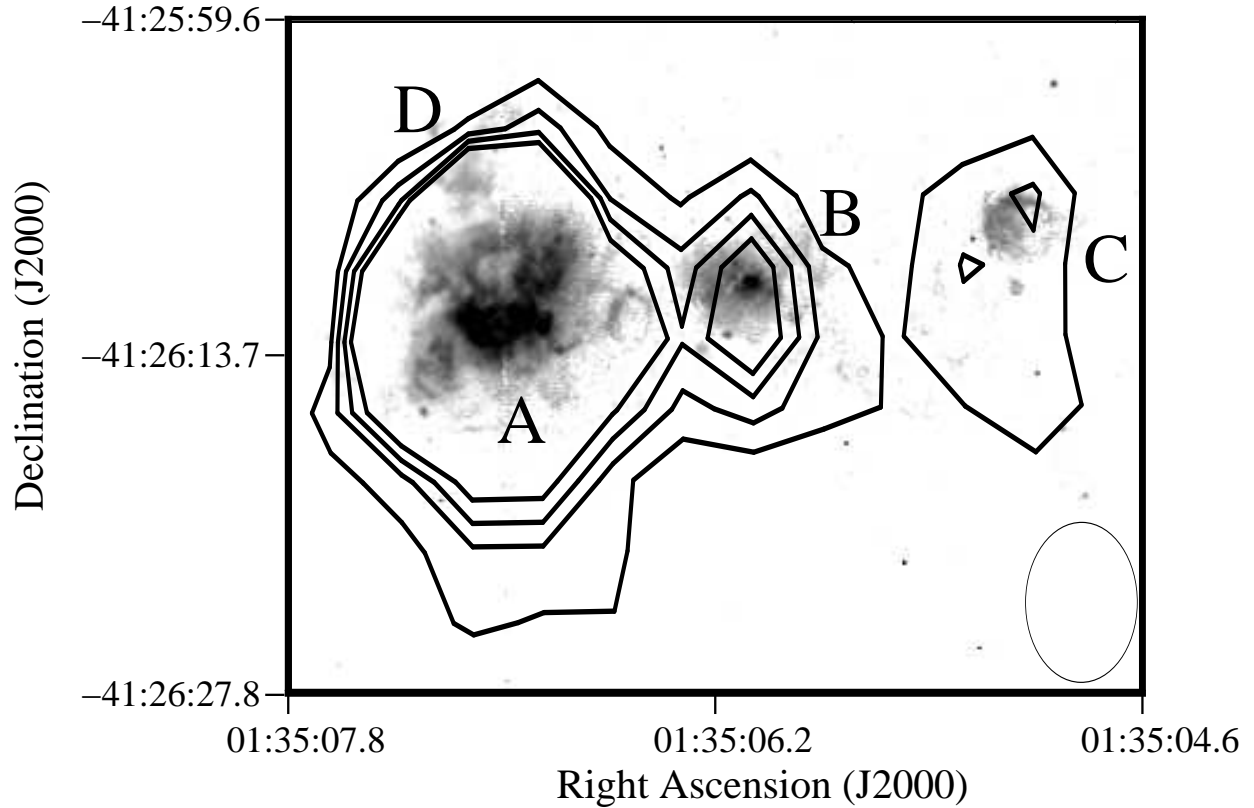


Fig. 6.— 1384 MHz continuum contours overlaid on a continuum-subtracted  $H\alpha$  image of NGC 625 (figure drawn from Cannon et al. 2003). Contours are at levels of 0.2, 0.3, 0.4, 0.5 mJy/Beam, corresponding to  $5$ ,  $7.5$ ,  $10$  and  $12.5\sigma$ . Labels A-D denote the nomenclature from Cannon et al. (2003); these complexes can be seen near the eastern end of the disk in Figure 1. The beam size is  $4.8'' \times 6.8''$  and is shown at the bottom right. The continuum luminosities of these H II regions are used in § 4 to estimate the reddening and contribution from non-thermal sources to the continuum luminosity.

Table 1. Basic Parameters of NGC 625

Property	Value	Reference
Distance (Mpc)	$3.89 \pm 0.22$	Cannon et al. (2003)
$M_B$	-16.3	Marlowe et al. (1997)
Gal. Lat. ( $^\circ$ )	-73.1	--
Foreground $A_V$ (mag.)	0.05	Schlegel et al. (1998)
$12 + \log(\text{O}/\text{H})$	$8.14 \pm 0.02$	Skillman et al. (2003b)
Current SFR ( $M_\odot \text{ yr}^{-1}$ )	0.05	Skillman et al. (2003a)
H I Mass ( $10^8 M_\odot$ )	$1.1 \pm 0.2$	This work
$V_{Helio}$ ( $\text{km s}^{-1}$ )	$413 \pm 5$	This work
$V_{20}$ ( $\text{km s}^{-1}$ )	$95 \pm 2$	This work
$V_{50}$ ( $\text{km s}^{-1}$ )	$62 \pm 2$	This work

Table 2. ATCA Observations of NGC 625

Array Configuration	Observation Date(s)	$T_{INT}$ (Minutes)
6 F	2001, 27 May	584
375	2001, 14, 16 Jun	176
1.5 A	2001, 15 Aug	579
6 B	2001, 19, 20 Aug	716
750 D	2001, 23 Sep	596
EW 352	2001, 11, 12, 13, 15, 17 Oct	1263
6 D	2001, 25 Nov, 4 Dec	606

Table 3. Radio Continuum vs. H $\alpha$  Comparison

H II Region(s) <sup>a</sup>	HST H $\alpha$ Flux <sup>b</sup> ( $10^{-14}$ erg sec $^{-1}$ cm $^{-2}$ )	T $_e$ <sup>c</sup> (K)	1384 MHz Flux Density (mJy)	Implied A $_{H\alpha}$ <sup>d</sup> (mag)	Optical A $_{H\alpha, Balmer}$ <sup>e</sup> (mag)
NGC 625 A+D	211 $\pm$ 10	10900 $^{+115}_{-109}$	7.5 $\pm$ 1.5	1.2 $\pm$ 0.5	0.27 $\pm$ 0.07
NGC 625 B	112 $\pm$ 6	10460 $^{+213}_{-193}$	1.2 $\pm$ 0.24	-0.2 $\pm$ 0.2	0.02 $\pm$ 0.09
NGC 625 C	7.8 $\pm$ 0.4	12810 $^{+460}_{-395}$	0.86 $\pm$ 0.17	2.2 $\pm$ 0.5	0.48 $\pm$ 0.09

<sup>a</sup>Adopting the nomenclature of Cannon et al. (2003); see Figure 6.

<sup>b</sup>Drawn from Cannon et al. (2003)

<sup>c</sup>Drawn from Skillman et al. (2003b)

<sup>d</sup>Calculated using H $\alpha$  values from Cannon et al. (2003) and the radio continuum values derived in this work.

<sup>e</sup>Applying spectroscopic  $c(H\beta)$  values from Skillman et al. (2003b), and the nomenclature of Bell et al. (2002).